Dynamic Rearrangement of Cell States Detected by Systematic Screening of Sequential Anticancer Treatments

Koplev, Simon; Longden, James; Ferkinghoff-Borg, Jesper; Bjerregård, Mathias Blicher; Cox, Thomas R.; Erler, Janine T.; Pedersen, Jesper T.; Voellmy, Franziska; Sommer, Morten Otto Alexander; Linding, Rune

Published in:
Cell Reports

Link to article, DOI:
10.1016/j.celrep.2017.08.095

Publication date:
2017

Document Version
Publisher's PDF, also known as Version of record

Cell Reports

Report

Dynamic Rearrangement of Cell States Detected by Systematic Screening of Sequential Anticancer Treatments

Graphical Abstract

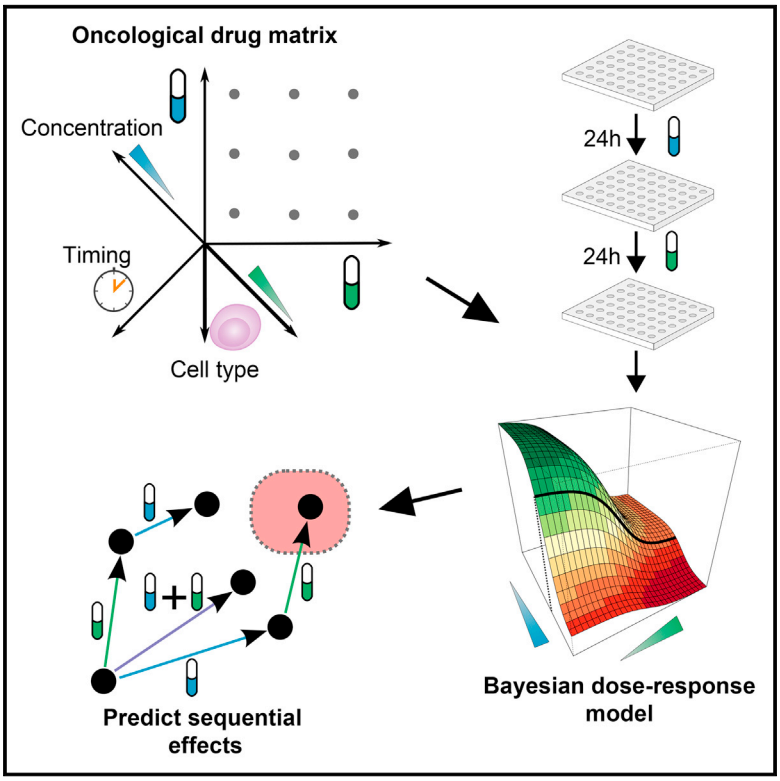

Highlights

- From an oncological drug matrix, we predicted sequentially effective drug combinations
- Approximately 23% of the 10,000 tested combinations showed sequential effects
- These findings demonstrate widespread time dependency of sequential drug combinations
- Responses were partially conserved between cancer cells of the same tissue origin

Authors

Simon Koplev, James Longden, Jesper Ferkinghoff-Borg, ..., Franziska Voellmy, Morten O.A. Sommer, Rune Linding

Correspondence

linding@lindinglab.org

In Brief

Therapeutic strategies, such as combination chemotherapy, rarely consider the timing of drug perturbations. Koplev et al. present a Bayesian dose-response framework for the prediction of sequentially effective drug combinations. They find widespread time dependency that is partially conserved between cancer cells of the same tissue origin.

Koplev et al., 2017, Cell Reports *20*, 2784–2791
September 19, 2017
http://dx.doi.org/10.1016/j.celrep.2017.08.095

CellPress

OPEN ACCESS
CellPress

Cell Reports
Report

Dynamic Rearrangement of Cell States Detected by Systematic Screening of Sequential Anticancer Treatments

Simon Koplev,[1,5] James Longden,[1,5] Jesper Ferkinghoff-Borg,[1,5] Mathias Blicher Bjerregård,[2] Thomas R. Cox,[3] Janine T. Erler,[1] Jesper T. Pedersen,[1] Franziska Voellmy,[1,4] Morten O.A. Sommer,[4] and Rune Linding[1,6,*]

[1]Biotech Research and Innovation Center, Faculty of Health and Medical Sciences, University of Copenhagen, Copenhagen 2200, Denmark
[2]DTU Compute, Technical University of Denmark, Kgs. Lyngby 2800, Denmark
[3]The Garvan Institute of Medical Research and The Kinghorn Cancer Centre, Faculty of Medicine, University of New South Wales, Sydney, NSW 2010, Australia
[4]Novo Nordisk Foundation Center for Biosustainability, Technical University of Denmark, Kgs. Lyngby 2800, Denmark
[5]These authors contributed equally
[6]Lead Contact
*Correspondence: linding@lindinglab.org
http://dx.doi.org/10.1016/j.celrep.2017.08.095

SUMMARY

Signaling networks are nonlinear and complex, involving a large ensemble of dynamic interaction states that fluctuate in space and time. However, therapeutic strategies, such as combination chemotherapy, rarely consider the timing of drug perturbations. If we are to advance drug discovery for complex diseases, it will be essential to develop methods capable of identifying dynamic cellular responses to clinically relevant perturbations. Here, we present a Bayesian dose-response framework and the screening of an oncological drug matrix, comprising 10,000 drug combinations in melanoma and pancreatic cancer cell lines, from which we predict sequentially effective drug combinations. Approximately 23% of the tested combinations showed high-confidence sequential effects (either synergistic or antagonistic), demonstrating that cellular perturbations of many drug combinations have temporal aspects, which are currently both underutilized and poorly understood.

INTRODUCTION

Combination therapies naturally extend the possible cellular perturbations that can be applied as treatment for diseased cells. It is known that the coordination of multiple drugs acting synergistically can improve therapeutic specificity (Lehár et al., 2009) and, for cancer, can increase the effectiveness of chemotherapy (DeVita et al., 1975; Chabner and Roberts, 2005). Thus, it is becoming increasingly evident that more complex treatment strategies will be required in order to remedy complex diseases and, in particular, to improve patient specificity.

Recently, several studies have reported time dependency of drug combinations—also known as schedule dependency, time staggering, sequence dependency, or simply sequential treatment. For example, erlotinib treatment in triple-negative breast cancer models has been shown to rewire an apoptosis-related signaling network, introducing a vulnerability to DNA damage by doxorubicin (Lee et al., 2012). In addition to time-dependent synergy, it has been shown that transient chemoresistance in breast cancer cells can be overcome by sequential treatment with taxanes followed by SFK/Hck inhibition (Goldman et al., 2015). Concurrent with these observations, nanoparticle delivery systems have been developed that provide the practical means for delivering small-molecule perturbations sequentially (Sengupta et al., 2005; Morton et al., 2014). Altogether, these provide compelling examples of how cellular dynamics can be exploited to increase cancer specificity, understand drug mechanisms, and overcome drug resistance.

Prior experiments assessing time dependency of anti-cancer drug combinations have typically been restricted to a small subset of drugs, timings, and cancer types. While hypothesis and candidate approaches can be useful systematic, high-throughput screening strategies provide a complimentary and unbiased approach for identifying combinatorial candidates (Al-Lazikani et al., 2012). To this end, we report a systematic cell-imaging screen and global Bayesian analysis of 10,000 sequential combinations of 100 United States Food and Drug Administration (FDA)-approved anti-cancer therapies in two cancer cell lines of melanoma and pancreatic origin. To assess cell-line specificity, we tested a subset of combinations in 4 additional pancreatic cancer cell lines. This represents the largest such screen to date, providing a collection of candidate combinations, along with experimental and analytical precedents for carrying out similar screens in other contexts.

RESULTS

Quantification of Cell Number following Treatment with Sequential Drug Combinations

Time-dependent synergy or antagonism can be viewed as sequential manipulations of cellular attractor states (Figure 1A). By measuring changes in cell number, we aimed to identify sequential drug combinations eliciting cytotoxic or proliferative

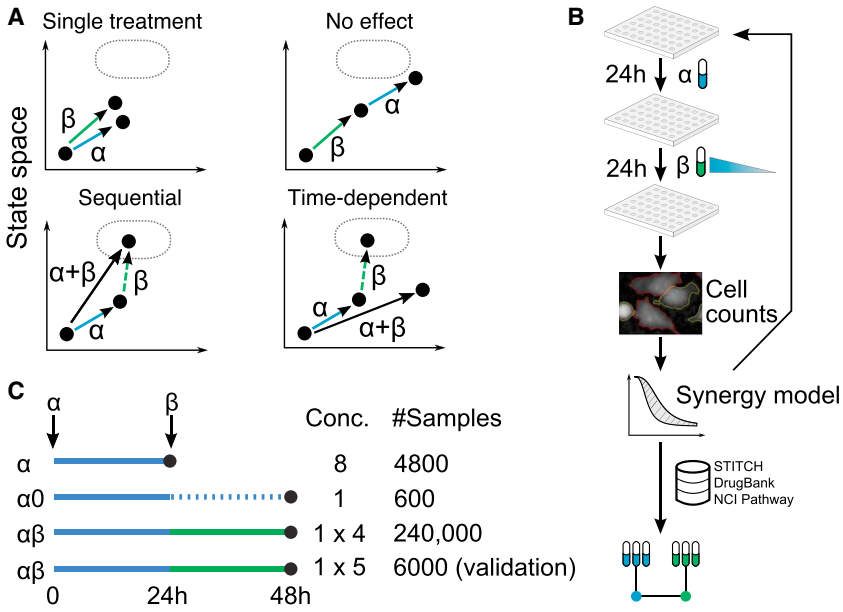

Figure 1. Systematic Screening of Sequential Combinations of Anticancer Drugs to Identify Temporal Synergy

(A) Schematic illustration of temporal synergy where changes in cell number can be induced by sequential treatment with drug α followed by drug β. Sequentially effective combinations could be time-dependent or reflect the dynamics of classical simultaneous synergy.

(B) Cytotoxicity measured by high-content imaging and quantified using a global synergy model, which prioritized additional validation experiments for 200 drug combinations. Cells, in 384-well plates, were treated with drug α for 24 hr and then treated with drug β for 24 hr at 4 doses. Common mechanisms explaining sequential synergy and antagonism across multiple drugs were then investigated.

(C) Experimental conditions for systematic screening of sequential combinations between 100 drugs, including timing and concentration series for 3 distinct types of experiments: drug α alone, in 8-point dose response, where cells were assayed after 24 hr; drug α0, where cells were treated with drug for 24 hr at 1 dose, and then the drug was removed and cells were assayed after 48 hr; and drug αβ, where cells were treated with 1 dose of drug α for 24 hr and then drug β in 4-point dose response (5-point dose response in the validation screen). All experiments were performed in triplicate, generating a total of ~250,000 data points.

states, which could inform about the dynamics of drug interactions, while providing candidates for time-dependent combinatorial treatment strategies.

A375 (malignant melanoma) and PANC1 (pancreatic adenocarcinoma) cells were treated with the 100 drugs that constitute the Approved Oncology Drug Set IV (Developmental Therapeutics Program, National Cancer Institute). Cells were exposed to single drugs in an 8-point dose-response curve. In separate experiments, cells were also exposed to sequential drug combinations where the first drug (α) was given at a single dose and the second drug (β) was given 24 hr later in a 4-point dose-response curve. Cell nuclei were then stained with Hoechst 33342 and imaged on the PerkinElmer Opera High-Content Screening System. Nuclei were quantified using the Acapella image analysis software (Figure 1B). Thus, for each of the 10,000 possible drug combinations, nuclei counts were measured after single-drug exposure (α0, αα, β0, and ββ) and sequential combination in both orders (αβ and βα) (Figure 1C). While simultaneous treatments were not directly measured, and thus cannot be definitively excluded, it is likely that order-specific observations (αβ versus βα) have some time dependency. All measurements were performed in triplicate, generating, in total, approximately 250,000 data points. These data represent an initial sparse screen, from which we selected 193 combinations with high synergy for validation experiments.

Global Bayesian Model of Pretreated Dose-Response Curves

To detect sequential effects of drug combinations, we took a global, probabilistic approach for modeling dose-response curves. First, the effects of sequential drug treatments were assumed to be Bliss independent (Al-Lazikani et al., 2012; Foucquier and Guedj, 2015), with a residual effect from the first drug, capturing delays in the effect on nuclei numbers (Figure 2A). This amounted to a 3-factor model capable of modeling both the single and combinatorial experiments. We then introduced the possibility for the combinatorial response curves of the second drug to deviate from the baseline response, which we used to define a synergy measure (Figure 1B). In total, the model consisted of 45,000 parameters, where inferential dependencies can be expressed as a Bayesian network (Figure S1A). We also assumed prior distributions for all parameters, which improved fitting convergence while avoiding overfitting. Finally, we modeled probability distributions over all parameters given both single and combinatorial drug experiments using Bayes's theorem.

Posterior probability distributions of the parameters were fitted using a Metropolis-Hastings algorithm—a Markov chain Monte Carlo (MCMC) method, which was run for 500,000 iterations with a burn-in period of 100,000 iterations and a 1/200 sample rate. Hence, each parameter fit consisted of 2,000 samples representing the uncertainty and posterior probabilities given all relevant nuclei count data. An example fit showing convergent parameter estimates is shown in Figure S1B. Based on this, we defined a "synergy measure" representing the average difference between the baseline and effective dose-response curve, where positive values indicated a synergistic interaction between drugs, and negative values indicated an antagonistic interaction (Figure 2B). The global nature and integrative structure of the model facilitated the testing of multiple hypotheses simultaneously. As such, each of the 10,100 dose-response curves could be viewed in the context of a subset of relevant data and parameters. This facilitated the drawing of cross-inferences, handled automatically through Bayesian inference. For example, Figure 2C illustrates the average posterior fits following

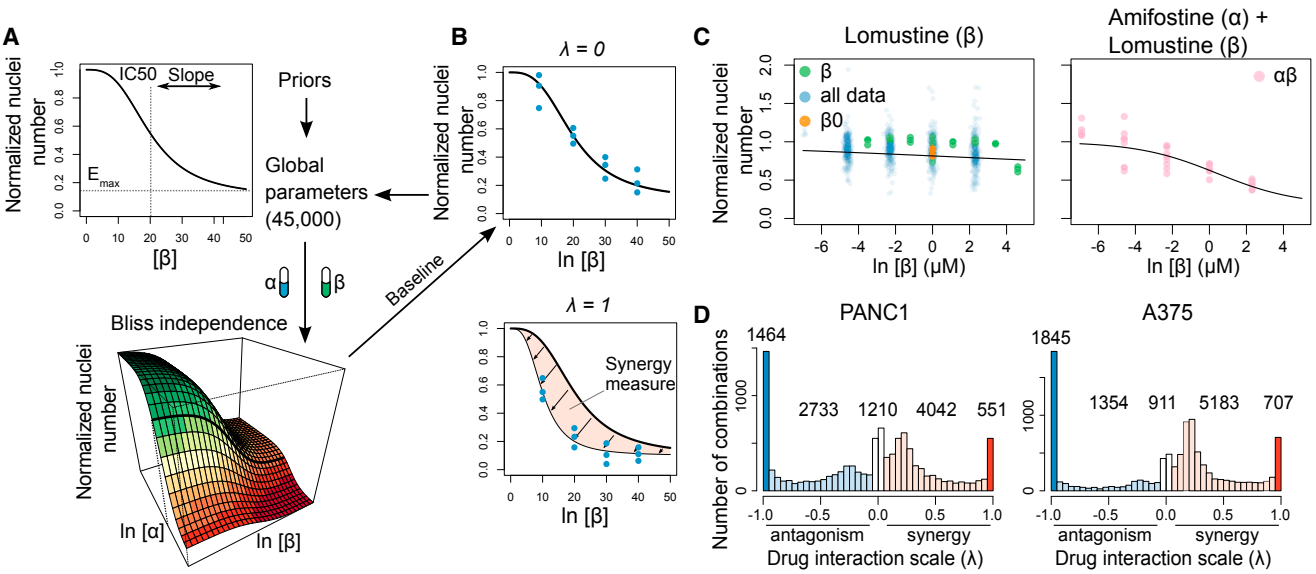

Figure 2. Global Bayesian Model of Cell Viability Data

(A) Global Bayesian model of cell viability data. In total, the model consisted of 45,000 parameters, over which posterior probability distributions were fitted using a Metropolis-Hastings algorithm, assuming sigmoidal dose-response curves and Bliss independence between consecutive treatments. Prior distributions over all parameters were assumed. Each observation of type α, $\alpha 0$, and $\alpha\beta$ carried equal weight in the Bayesian inference.

(B) Special selector variables (λ) were used to enable the $\alpha\beta$ data to influence the baseline fit for a more conservative estimate of sequential effects. Synergy was quantified as the difference between the expected baseline and the model fit, with antagonism associated with negative values of this measure.

(C) Example of validated model fit in A375. Left: conservative fit of baseline dose-response curve for lomustine based on average posterior parameters from supporting data points, including controls (experiment types β and $\beta 0$) in addition to all combinatorial experiments ($\alpha\beta$) that involved lomustine. To illustrate their influence on the baseline fit, each point was scaled by effects from residuals and non-lomustine drugs according to the 3-factor Bliss independence model. Right: average fitted dose-response curve for lomustine pretreated with amifostine, showing a synergistic sequential effect, $p < 0.0005$.

(D) Distribution of the posterior MCMC frequencies of selector variables for all 10,000 sequential combinations estimating the likelihood of drug interaction and whether the interaction was synergistic or antagonistic. These "λ scores" were multiplied by -1 for antagonistic combinations yielding a range of $[-1, 1]$, where -1 corresponds to the most antagonistic combination and +1 corresponds to the most synergistic combination.

treatment of A375 cells with lomustine alone and amifostine followed by lomustine. The model utilized a combination of data from single-drug and combinatorial treatments to fit the baseline dose-response curves. In this way, the inherent biological and technical variations inherent in the assay were taken into account, resulting in more conservative estimates of sequential effects; in this case, that amifostine pretreatment was synergistic with lomustine.

Sequential Effects Are Mostly Time-Dependent and Cell-Line-Specific

The global dose-response model identified 1,258 synergistic drug combinations ($p < 0.05$; 551 in PANC1 and 707 in A375) and 3,309 antagonistic combinations ($p < 0.05$; 1,464 in PANC1 and 1,845 in A375); in total, approximately 23% of all combinations tested (Figures 2D and S2). The temporal synergy measures of PANC1 and A375 were weakly correlated ($r = 0.19$, Pearson's correlation), with the majority of the correlation observed in the antagonistic domain. This is, perhaps, unsurprising given the different origins of the two cell lines tested.

To better assess the cell-line specificity of the sequential effects, we screened a subset of 193 drug combinations in four pancreatic cancer cell lines: AsPC-1, BXPC3, Capan1, and DAN-G (Figures S3A and S3B). The majority of the concordant drug interactions were, again, found in the antagonistic domain; overall, the correlations with PANC1 were higher than for the melanoma cell line, ranging from $r = 0.50$ to $r = 0.67$ (Pearson's correlation; Figure S3C). While PANC1 was more correlated to the other pancreatic cancer cell lines than it was to A375, Capan1 and AsPC-1 were even more highly correlated ($r = 0.74$), as were DAN-G and BXPC3 ($r = 0.81$). There does not appear to be an obvious genomic explanation for these observations; however, DAN-G and BXPC3 had similar growth characteristics in this screen, proliferating significantly faster than Capan-1 and AsPC-1 (doubling times of 1 to 1.5 days for DAN-G and BXPC3 versus 2 to 3 days for Capan-1 and AsPC-1). These observations suggest that cell lines broadly respond differently to sequential treatment, yet some drug-driven network state changes may be conserved between cells of similar phenotype. Further investigations in more, well-characterized cell lines would be required to determine whether this observation has clinical relevance, yet it may suggest a potential role for patient-derived xenograph models in order to identify patient-specific temporal combinations.

We also compared reversed treatments in each cell line (e.g., $\alpha\beta$ versus $\beta\alpha$) in order to discern whether the identified sequential effects were time-dependent. For all reversed

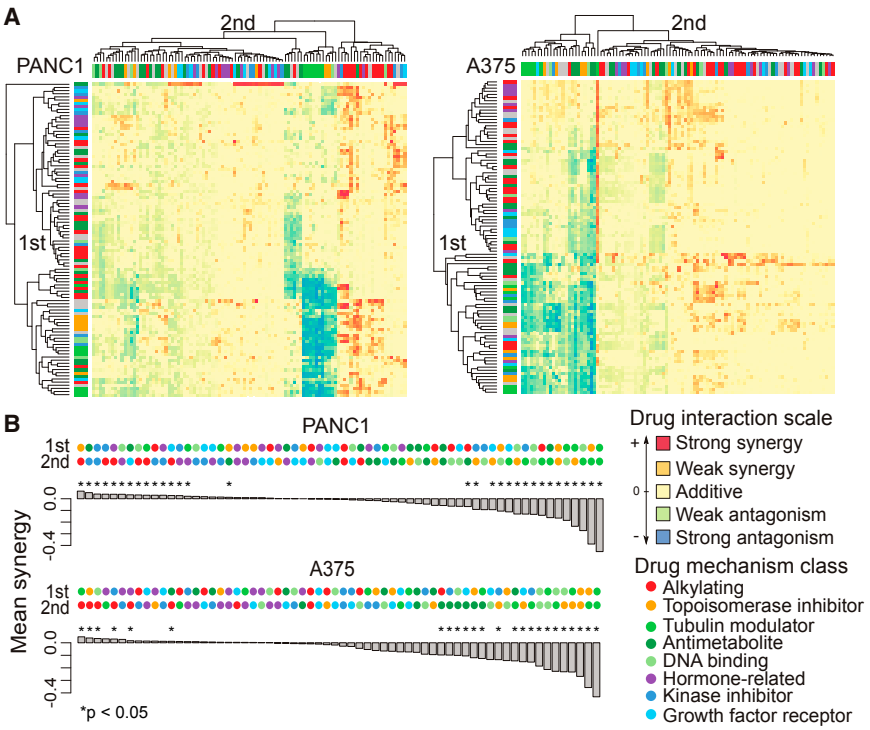

Figure 3. Sequential Synergism and Antagonism among Anticancer Drugs Are Common in A375 and PANC1 Cell Lines

(A) Heatmaps of average posterior synergy measures (difference from baseline) for all 10,000 sequential combinations tested in PANC1 and A375, where blue indicates strong antagonism and red indicates strong synergy. Rows and columns correspond to first and second drugs, are arranged by hierarchical clustering, and are colored by classes of drug mechanisms.

(B) Average synergy measure by drug mechanism showing, in both cell lines, increased synergy following secondary treatment with alkylating agents and strong antagonism following secondary treatment with tubulin modulators. Significance was assessed by permutation tests.

combinations, synergy measures were only weakly correlated for both A375 (r = 0.25) and PANC1 (r = 0.23), concordant with widespread time dependency of sequential drug combinations.

Iterative Model Improvement and Validation Increase the Discovery Rate

Model-based experimentation is known to increase the search efficiency for combinatorial treatments; by first performing a sparse screen and then conducting additional experiments in selected regions, positive results are more likely to be found (Creixell et al., 2012; Janes and Yaffe, 2006). Accordingly, based on preliminary model predictions of highly synergistic and antagonistic drug combinations, we carried out validation experiments for 192 drug combinations in each cell line where the first drug was given at a single dose and the second drug was given 24 hr later in 5-point dose response. Overall, we found the model predictions to be reproducible (Figure S4A), even though the selected top combinations represent a worst-case validation, with any experimental outliers having a disproportional effect on the model fit. These validation results were used to further refine the model so that the updated synergy measures, presented throughout this study, take into account both the primary screen and validation data.

Drug Mechanisms Predict Temporal Synergy and Antagonism

Clustering the first and second drugs by their synergy measures identified clusters of synergy and antagonism (Figure 3A) that associated with broad classes of drug mechanisms collated from DrugBank (Law et al., 2014). Most prominently, antagonistic drug clusters associated with secondary tubulin modulator treatment (Figures 3B). This time-dependent antagonistic interaction between tubulin modulators and other drugs has been previously reported (Vanhoefer et al., 1995; Xiong et al., 2007) and suggested to be cell-cycle-dependent. In addition, we found a synergistic tendency for secondary treatment with alkylating drugs (Figure 3B), which corroborates previous findings of induced sensitivity to DNA damage (Lee et al., 2012).

In addition to drug mechanisms, we investigated whether synergy measures clustered by protein targets (Kuhn et al., 2014) and National Cancer Institute pathway associations (Schaefer et al., 2009). Drug combinations with shared targets (Law et al., 2014) were more likely to be antagonistic (Figure S4B), indicating that using drug target overlap to propose novel sequential combinations in silico (Zhao et al., 2011) may be prone to adaptive cellular responses. In cross-validated predictions of synergy measures, drug mechanism was consistently the most predictive, with the inclusion of protein targets and pathways further increasing predictive power (Figure 4A). By including all model components that improved cross-validation performance (Figure 4A), regression coefficients were used to dissect molecular mechanisms underlying sequential synergy and antagonism in terms of protein targets, pathways, and mechanisms (Figure 4B).

These observations suggest that drug annotations of combinatorial treatments are predictive of sequential synergy and antagonism. This may, in turn, indicate that drugs inducing similar states possibly reflect shared dynamic mechanisms. It should, thus, be expected that functional efforts to better characterize the dynamics of drug perturbations would enable more precise models of sequential treatments.

DISCUSSION

The systematic screen and global statistical model described here effectively identified synergistic, time-dependent temporal

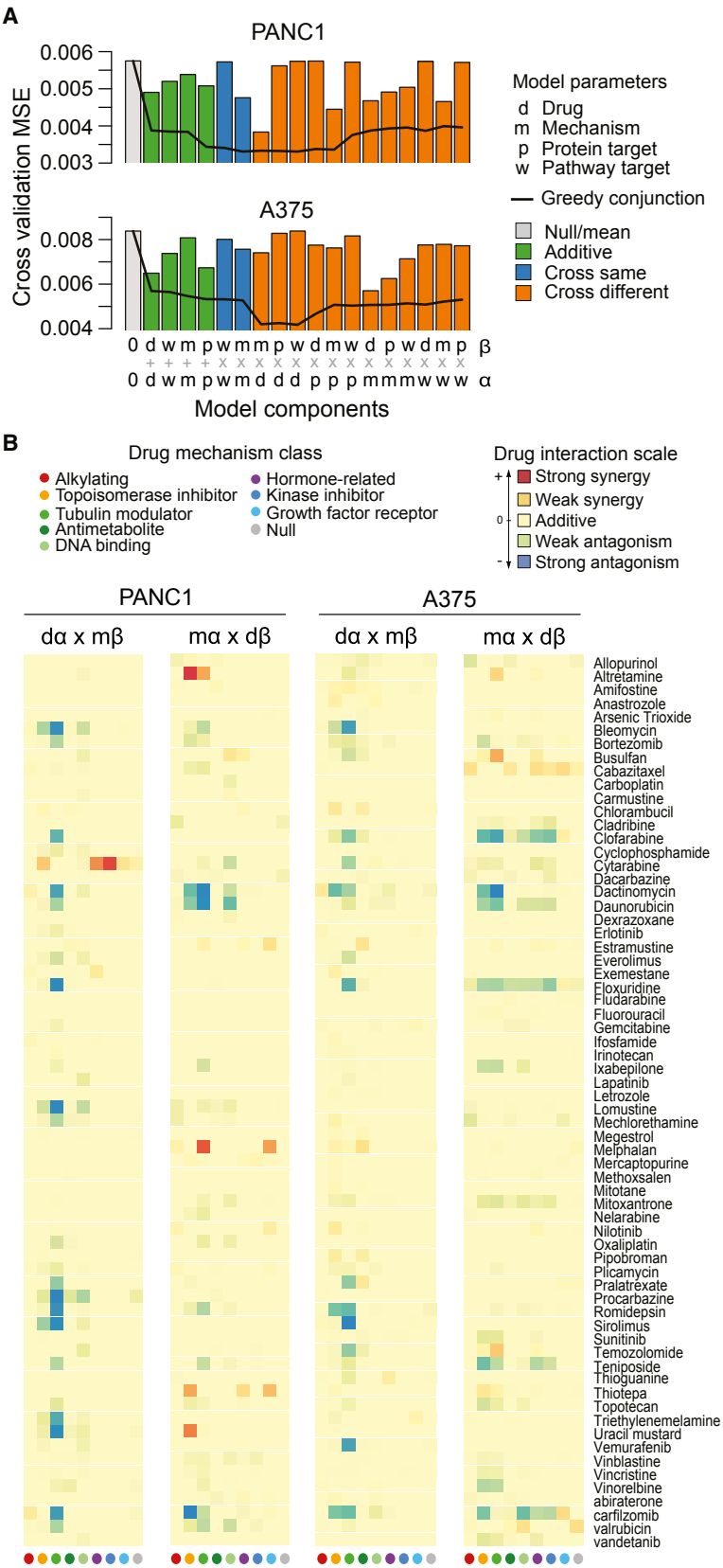

Figure 4. Regression-Based Interpretation of Schedule-Dependent Synergy in Terms of Drug Mechanisms, Protein Targets, and Associated Molecular Pathways

(A) Cross-validation error of classes of regression models for the first (α) and second (β) drugs, illustrating that drug protein targets and/or pathway activity did not significantly improve predictive power over mechanism alone. However, some particular meta-features, such as the protein target of the pretreatment combined with the mechanism of the secondary treatment, did increase predictive power. The line represents the greedy conjunction of the best performing models added one at a time in the order of their individual cross-validation performance. All fits were controlled for overfitting by using the hyperparameter value yielding the lowest 10-fold cross-validation error.

(B) Mean synergy measures quantified by repression coefficients illustrating synergistic and antagonistic effects from individual drugs and drugs grouped according to their described mechanism, as either the first (α) or the second (β) treatment.

treatments in cancer cell lines. Factors contributing to this efficiency include the use of Bayesian statistics and a strategy of sparse systematic experimentation followed by model-based follow-up experiments and validation. To our knowledge, it has not previously been shown that a global probabilistic model for drug combinations would be a practical analysis scheme. Hence, that such a model was algorithmically feasible was a remarkable result in itself.

Alternative methods for quantifying drug synergy, such as the Chou-Talalay Combination Index (Chou and Talalay, 1984), assume dose equivalence, which is invalid when drugs are not administered simultaneously. In contrast, the sequential Bliss independence model used here does not assume dose equivalence but allows for self-synergy and antagonism, the meaning of which is related to sustained drug treatment but not strictly a combinatorial synergy or antagonism. For these reasons, classical theory of synergism must be handled carefully for sequential treatment.

Using this model, we have identified several time-dependent combinations that could potentially have clinical relevance. The finding that amifostine pretreatment is synergistic with lomustine was noteworthy, since amifostine was originally designed as a cytoprotectant, reducing kidney damage from cisplatin (Kouvaris et al., 2007). However, it has now been shown that amifostine has a complex mechanism of action that can mimic hypoxia and promote vascular endothelial growth factor expression (Dedieu et al., 2010). It is, therefore, not surprising that it could, in a time-dependent manner, promote the efficacy of other drugs in some cellular contexts.

Clinical trials have shown improved survival in patients with pancreatic cancer following treatment with gemcitabine and cisplatin (Ouyang et al., 2016), a well-established synergistic combination (Bergman et al., 1996), and gemcitabine and capecitabine (Neoptolemos et al., 2016), combinations that were both found to be synergistic in this study. In the case of gemcitabine and cisplatin, we found equal synergy regardless of treatment order (gemcitabine then cisplatin: $\lambda = 0.724$; and cisplatin then gemcitabine: $\lambda = 0.805$) and self-synergy for cisplatin alone ($\lambda = 0.735$). In contrast, gemcitabine was found to be highly self-antagonistic ($\lambda = -1$). For the combination of gemcitabine and capecitabine, synergy was only observed when gemcitabine was administered first ($\lambda = 0.69$). These examples illustrate cases of classical synergy with and without time dependency of sequential application. Recently, sequential application of gemcitabine, followed by erlotinib 18–24 hr later, has been shown to be efficacious in in vitro models of pancreatic cancer (Ubezio et al., 2016). Our study supports this finding, with gemcitabine followed by erlotinib found to be highly synergistic in PANC1 cells ($\lambda = 0.996$). While gemcitabine and erlotinib combination therapies have shown some efficacy in the clinic (Moore et al., 2007), the effect of sequential applications of these drugs is yet to be determined.

For malignant melanoma, combinations of bortezomib and vemurafenib have previously been reported to be synergistic in a panel of 7 melanoma cell lines (Bolomsky et al., 2013). Our model validated this synergistic effect, but only when bortezomib was given first ($\lambda = 0.926$). If vemurafenib was given first, the combination was, instead, highly antagonistic ($\lambda = -1$), as was bortezomib alone ($\lambda = -1$). Interestingly, we also noted a synergistic effect from combinations of erlotinib and vemurafenib, if erlotinib was given first ($\lambda = 0.725$). It is well known that vemurafenib resistance in colon cancer is driven by feedback activation of the epidermal growth factor receptor (EGFR) and that combination therapies of vemurafenib and erlotinib are, thus, synergistic in both in vitro and in vivo models (Prahallad et al., 2012). Melanoma cells, however, usually express low levels of EGFR, but this is not the case for A375, which has relatively high EGFR expression (Mirmohammadsadegh et al., 2007), and a subset of human tumors (Sun et al., 2014). Therefore, the dynamics of EGFR inhibition by erlotinib in A375 might explain the sensitization to subsequent treatment with vemurafenib in this study.

Temporal order is rarely considered when designing clinical trials and optimal treatment schedules for combination therapies, yet the results presented here, and in other more focused studies, clearly show that sequential synergy and antagonism are common and highly time-dependent among approved anticancer therapies. It is, thus, becoming increasingly clear that time-dependent synergy is a crucial consideration to maximize efficacy and that time-dependent antagonism could be particularly important to avoid resistance.

Our understanding of adaptation, compensation, and network rewiring is currently insufficient to allow accurate ab initio predictions of the cellular response in any cell type. However, once we unravel how cells rewire and reach new network states, it will be feasible to attempt to force tumor cells out of these states in order to kill or "normalize" them through drug-induced dynamic rewiring of signaling networks.

EXPERIMENTAL PROCEDURES

Further details and an outline of resources used in this work can be found in the Supplemental Experimental Procedures.

Dose-Response Parameterization and Priors

Individual cell viabilities were modeled according to classical sigmoidal drug-response curves, where a parameter, K, represents the inverse of half of the maximal inhibitory concentration (IC_{50}), h determines slope, and α represents the maximum effect on cell viability. The global model consisted of dose-response curve parameters for each of the 100 small-molecule compounds and for each of the 10,000 sequential combinations. Cell growth was assumed to be a discrete two-step process with residual effect from the first treatment during the second treatment. Assuming Bliss independence, the baseline response was, thus, considered a product of 3 factors: the viability effects of the first and second drugs and the residual effect of the first drug. Selector variables were defined as Boolean variables, which determined whether the combinatorial effect is explained by the single-drug parameters or by a new set of parameters modeling the synergy or antagonism.

The precision of the cell counts ($variance^{-1}$) was assumed to follow a Gamma distribution. Hence, the sufficient statistics—namely, the experimental mean and variance of normalized cell counts across experimental repeats—were used to fit the model parameters. For the global Bayesian curve fit, we assumed the following prior probability distributions: K, ~log N(0.1, 0.2); h, ~log N(1.5, 2.0); α, ~beta(1, 3); ε, ~gamma(0.6, 0.02), where ε is the cell-count precision. All concentration-specific parameters were expressed in micromolar amounts.

Estimation of Posterior Distribution

To evaluate the posterior density of the model parameters given the observed data, we simulated a chain of complete parameter sets according to a modified Metropolis-Hastings algorithm. We used a modified Gibbs sampling

procedure for proposal distribution, where, at each iteration, proposals were made independently for curve parameter sets and the associated selector variable. For calculating the Metropolis-Hastings acceptance ratios, we considered proposals of 4 cases based on the previous and proposed selector variables. This simplified the proposal correction for the Metropolis-Hastings acceptance ratios under particular choices of proposal distributions, enabling a scheme where curve parameters were only explored if a selector variable remains on.

For the parameters K, h, and α, we used Gaussian proposal distributions, with reject for negative outcomes and SDs 2.0, 0.5, and 3.0, respectively. For each curve parameter set, the selector variable was drawn from a Bernoulli distribution with 0.1 probability of switching state. If the selector variable remained on, then 1 out of 3 parameters was chosen randomly for proposal as described. The MCMC simulation was implemented in C++11 using the < random > library for sampling numbers following the described probability distributions. At every 200th iteration of parameters, sets were sampled after a burn-in period of 100,000 and for a total of 500,000 iterations. Finally, an aggregate synergy measure was evaluated as the average area between the baseline and combined dose-response curves along with λ, defined as the average value of the selector variable for each drug combination.

Data and Software Availability

The source code for the program fitting sequential, combinatorial dose-response curves through MCMC samples from the posterior distribution is available at the following URL, under a GNU General Public License Version 3: https://github.com/skoplev/d-chain.

Additional documentation can be found at https://dchain.lindinglab.org.

Aggregate model data from the combinatorial and validation screens can be found at: http://dx.doi.org/10.17632/wgybvcvjwf.1.

SUPPLEMENTAL INFORMATION

Supplemental Information includes Supplemental Experimental Procedures and four figures and can be found with this article online at http://dx.doi.org/10.1016/j.celrep.2017.08.095.

AUTHOR CONTRIBUTIONS

Conceptualization, R.L. and M.O.A.S.; Methodology, S.K., J.L., J.F.-B., M.B.B., and J.T.E.; Investigation, J.L., T.R.C., J.T.P., and F.V.; Writing – Original Draft, S.K., J.L., and R.L.; Writing – Review and Editing, S.K., J.L., and R.L.; Supervision, J.L., J.F.-B., M.O.A.S., and R.L.; Funding Acquisition, R.L.

ACKNOWLEDGMENTS

This work was funded by a Lundbeck Foundation Junior Group Leader Fellowship (2011-7290). The compound library was obtained from the National Cancer Institute/Division of Cancer Treatment and Diagnosis (DCTD)/Developmental Therapeutics Program (DTP) (http://dtp.cancer.gov). Drug screening was performed using the Villum Fonden Center for Systems Proteomics (VKR 022758).

Received: May 21, 2017
Revised: August 25, 2017
Accepted: August 29, 2017
Published: September 19, 2017

REFERENCES

Al-Lazikani, B., Banerji, U., and Workman, P. (2012). Combinatorial drug therapy for cancer in the post-genomic era. Nat. Biotechnol. *30*, 679–692.

Bergman, A.M., Ruiz van Haperen, V.W., Veerman, G., Kuiper, C.M., and Peters, G.J. (1996). Synergistic interaction between cisplatin and gemcitabine in vitro. Clin. Cancer Res. *2*, 521–530.

Bolomsky, A., Ludwig, H., and Zojer, N. (2013). Vemurafenib inhibits myeloma cell growth independent of BRAF V600E mutations, potentiates the activity of established anti-myeloma drugs, but impairs osteogenesis via an HGF autocrine loop in bone marrow stromal cells. Blood *122*, 5363.

Chabner, B.A., and Roberts, T.G., Jr. (2005). Timeline: Chemotherapy and the war on cancer. Nat. Rev. Cancer *5*, 65–72.

Chou, T.C., and Talalay, P. (1984). Quantitative analysis of dose-effect relationships: the combined effects of multiple drugs or enzyme inhibitors. Adv. Enzyme Regul. *22*, 27–55.

Creixell, P., Schoof, E.M., Erler, J.T., and Linding, R. (2012). Navigating cancer network attractors for tumor-specific therapy. Nat. Biotechnol. *30*, 842–848.

Dedieu, S., Canron, X., Rezvani, H.R., Bouchecareilh, M., Mazurier, F., Sinisi, R., Zanda, M., Moenner, M., Bikfalvi, A., and North, S. (2010). The cytoprotective drug amifostine modifies both expression and activity of the pro-angiogenic factor VEGF-A. BMC Med. *8*, 19.

DeVita, V.T., Jr., Young, R.C., and Canellos, G.P. (1975). Combination versus single agent chemotherapy: a review of the basis for selection of drug treatment of cancer. Cancer *35*, 98–110.

Foucquier, J., and Guedj, M. (2015). Analysis of drug combinations: current methodological landscape. Pharmacol. Res. Perspect. *3*, e00149.

Goldman, A., Majumder, B., Dhawan, A., Ravi, S., Goldman, D., Kohandel, M., Majumder, P.K., and Sengupta, S. (2015). Temporally sequenced anticancer drugs overcome adaptive resistance by targeting a vulnerable chemotherapy-induced phenotypic transition. Nat. Commun. *6*, 6139.

Janes, K.A., and Yaffe, M.B. (2006). Data-driven modelling of signal-transduction networks. Nat. Rev. Mol. Cell Biol. *7*, 820–828.

Kouvaris, J.R., Kouloulias, V.E., and Vlahos, L.J. (2007). Amifostine: the first selective-target and broad-spectrum radioprotector. Oncologist *12*, 738–747.

Kuhn, M., Szklarczyk, D., Pletscher-Frankild, S., Blicher, T.H., von Mering, C., Jensen, L.J., and Bork, P. (2014). STITCH 4: integration of protein-chemical interactions with user data. Nucleic Acids Res. *42*, D401–D407.

Law, V., Knox, C., Djoumbou, Y., Jewison, T., Guo, A.C., Liu, Y., Maciejewski, A., Arndt, D., Wilson, M., Neveu, V., et al. (2014). DrugBank 4.0: shedding new light on drug metabolism. Nucleic Acids Res. *42*, D1091–D1097.

Lee, M.J., Ye, A.S., Gardino, A.K., Heijink, A.M., Sorger, P.K., MacBeath, G., and Yaffe, M.B. (2012). Sequential application of anticancer drugs enhances cell death by rewiring apoptotic signaling networks. Cell *149*, 780–794.

Lehár, J., Krueger, A.S., Avery, W., Heilbut, A.M., Johansen, L.M., Price, E.R., Rickles, R.J., Short, G.F., 3rd, Staunton, J.E., Jin, X., et al. (2009). Synergistic drug combinations tend to improve therapeutically relevant selectivity. Nat. Biotechnol. *27*, 659–666.

Mirmohammadsadegh, A., Mota, R., Gustrau, A., Hassan, M., Nambiar, S., Marini, A., Bojar, H., Tannapfel, A., and Hengge, U.R. (2007). ERK1/2 is highly phosphorylated in melanoma metastases and protects melanoma cells from cisplatin-mediated apoptosis. J. Invest. Dermatol. *127*, 2207–2215.

Moore, M.J., Goldstein, D., Hamm, J., Figer, A., Hecht, J.R., Gallinger, S., Au, H.J., Murawa, P., Walde, D., Wolff, R.A., et al.; National Cancer Institute of Canada Clinical Trials Group (2007). Erlotinib plus gemcitabine compared with gemcitabine alone in patients with advanced pancreatic cancer: a phase III trial of the National Cancer Institute of Canada Clinical Trials Group. J. Clin. Oncol. *25*, 1960–1966.

Morton, S.W., Lee, M.J., Deng, Z.J., Dreaden, E.C., Siouve, E., Shopsowitz, K.E., Shah, N.J., Yaffe, M.B., and Hammond, P.T. (2014). A nanoparticle-based combination chemotherapy delivery system for enhanced tumor killing by dynamic rewiring of signaling pathways. Sci. Signal. *7*, ra44.

Neoptolemos, J.P., Palmer, D., Ghaneh, P., Valle, J.W., Cunningham, D., Wadsley, J., Meyer, T., Anthoney, A., Glimelius, B., Falk, S., et al. (2016). ESPAC-4: A multicenter, international, open-label randomized controlled phase III trial of adjuvant combination chemotherapy of gemcitabine (GEM) and capecitabine (CAP) versus monotherapy gemcitabine in patients with resected pancreatic ductal carcinoma. J. Clin. Oncol. *34*, LBA4006.

Ouyang, G., Liu, Z., Huang, S., Li, Q., Xiong, L., Miao, X., and Wen, Y. (2016). Gemcitabine plus cisplatin versus gemcitabine alone in the treatment of pancreatic cancer: a meta-analysis. World J. Surg. Oncol. *14*, 59.

Prahallad, A., Sun, C., Huang, S., Di Nicolantonio, F., Salazar, R., Zecchin, D., Beijersbergen, R.L., Bardelli, A., and Bernards, R. (2012). Unresponsiveness of colon cancer to BRAF(V600E) inhibition through feedback activation of EGFR. Nature *483*, 100–103.

Schaefer, C.F., Anthony, K., Krupa, S., Buchoff, J., Day, M., Hannay, T., and Buetow, K.H. (2009). PID: the Pathway Interaction Database. Nucleic Acids Res. *37*, D674–D679.

Sengupta, S., Eavarone, D., Capila, I., Zhao, G., Watson, N., Kiziltepe, T., and Sasisekharan, R. (2005). Temporal targeting of tumour cells and neovasculature with a nanoscale delivery system. Nature *436*, 568–572.

Sun, C., Wang, L., Huang, S., Heynen, G.J.J.E., Prahallad, A., Robert, C., Haanen, J., Blank, C., Wesseling, J., Willems, S.M., et al. (2014). Reversible and adaptive resistance to BRAF(V600E) inhibition in melanoma. Nature *508*, 118–122.

Ubezio, P., Falcetta, F., Carrassa, L., and Lupi, M. (2016). Integrated experimental and simulation study of the response to sequential treatment with erlotinib and gemcitabine in pancreatic cancer. Oncotarget *7*, 15492–15506.

Vanhoefer, U., Harstrick, A., Wilke, H., Schleucher, N., Walles, H., Schröder, J., and Seeber, S. (1995). Schedule-dependent antagonism of paclitaxel and cisplatin in human gastric and ovarian carcinoma cell lines in vitro. Eur. J. Cancer *31A*, 92–97.

Xiong, X., Sui, M., Fan, W., and Kraft, A.S. (2007). Cell cycle dependent antagonistic interactions between paclitaxel and carboplatin in combination therapy. Cancer Biol. Ther. *6*, 1067–1073.

Zhao, X.-M., Iskar, M., Zeller, G., Kuhn, M., van Noort, V., and Bork, P. (2011). Prediction of drug combinations by integrating molecular and pharmacological data. PLoS Comput. Biol. *7*, e1002323.